# Study of Triple Ar Gas Puff Z-Pinches on 0.9-MA, 200-ns COBRA

N. Qi, S. V. Rocco, J. Engelbrecht, E. S. Lavine, P. de Grouchy, J. T. Banasek, L. Atoyan, T. Byvank, W. M. Potter, J. B. Greenly, D. A. Hammer, B. R. Kusse, S. A. Pikuz, T. A. Shelkovenko, E. Kroupp, A. Fisher, and Y. Maron

***Abstract*— Ar gas puff z-pinch experiments were conducted on the 0.9-MA, 200-ns COBRA generator at Cornell University. In the experiments, a triple-nozzle gas valve was used to produce the z-pinch load with concentric outer and inner gas puffs and a central gas jet. We used a planer laser-induced fluorescence to measure the initial gas profile of the load, two four-frame 4-ns gated extreme ultraviolet cameras to image the imploding plasma, and filtered photoconducting diamond detectors to measure the X-ray output. We have observed the shock heating and/or photoionization of the dense center jet by the imploding plasma. With an outer-to-inner plenum pressure ratio of 1:3, deacceleration of the imploding plasma occurred when the outer plasma shell imploded on the inner shell resulting in a stable implosion. By varying the plenum pressure for the center jet, the X-ray emission was optimized. An Ar K-shell X-ray (3–4 keV) yield of 77 ± 17 J was produced at a current level of 0.87 ± 0.2 MA and an implosion time of 200 ns.**

***Index Terms*— K-shell radiation production, plasma radiation source, z-pinch plasmas.**

## I. Introduction

Dense z-pinch plasmas are high power, energy-efficient laboratory sources of X-rays with photon energies ranging from hundreds of electronvolts to several kiloelectronvolts [1]–[4]. The loads of these plasma radiation sources are either wire arrays or gas puffs. They have been widely investigated with short implosion times (≈100 ns) [5]–[10]. Longer implosion time (>200 ns) z-pinches have several advantages; reduced voltage, more stored energy, and significantly less expensive pulsed power drivers. For this paper, we make a distinction between the implosion time and the rise time of the pulse power driver. The implosion time is the time it takes the imploding, pinched plasma to reach stagnation on the cylindrical axis. The rise time of the pulsed power driver is the time it takes the driver current to reach its peak value. For "stiff" low-impedance drivers, these times are essentially independent. The most efficient transfer of energy to the stagnated, pinched plasma occurs when these times are approximately equal.

In high-current z-pinches, the electrical power is delivered to the loads through magnetically insulated transmission lines (MITL). The slower pulsed power drivers (200 ns) that are used for the longer implosion times operate at a lower voltage for a given peak current than the fast drivers (100 ns). These lower voltage drivers are less expensive than the faster ones and also have a less current loss in the MITL [11].

For intense K-shell X-ray radiation, a sufficient ion kinetic energy is needed in order to reach the K-shell ionization state. In a single-shell gas puff z-pinch, the ion stagnation velocity is proportional to the initial z-pinch radius divided by the implosion time. Consequently, long implosion time (200 ns) z-pinches have to use large diameter loads. This increases the compressing ratio of the implosions. Higher compression ratio z-pinches enable more energy to be coupled to the load, and produce high kinetic energy in ions. Longer implosion times have an advantage for delivering more energy to the load to produce K-shell radiation. However, for long implosion times, the magnetic Rayleigh–Taylor (MRT) instability problem becomes more serious. The MRT instability growth rate is given by $(kg\ t^2)^{0.5} \approx (0.5\ kR)^{0.5}$, where $k$ is the MRT instability wavelength, $g$ is the plasma acceleration, and $R$ is the initial plasma radius. Thus, it grows exponentially as the square root of the load diameter. When the implosion time is doubled, the load diameter is also doubled. The MRT instability would result in a fatter, stagnated plasma column (lower implosion compression ratio) and a ∼50% reduction of the X-ray yields for the 200-ns implosions as it has observed in past experiments [12]. To minimize the problems caused by the MRT instability for ∼200-ns implosions, it has been suggested to use a tailored radial distribution for the initial gas puff [13]. During the implosion with the outer and inner gas puff, the plasma experiences an acceleration, then a deceleration, and then finally another acceleration. In the deceleration phase, the

Manuscript received January 15, 2018; revised July 17, 2018 and September 24, 2018; accepted September 28, 2018. Date of publication October 22, 2018; date of current version November 8, 2018. This work was supported by the National Nuclear Security Administration Stewardship Sciences Academic Programs through the Department of Energy Cooperative Agreement under Grant DE-NA0001836. The review of this paper was arranged by Senior Editor F. Beg. *(Corresponding author: N. Qi.)*

N. Qi is with the Laboratory of Plasma Studies, Cornell University, Ithaca, NY 14853 USA, and also with L-3 Applied Technologies, Inc., San Leandro, CA 94577 USA (e-mail: nq27@cornell.edu).

S. V. Rocco, E. S. Lavine, P. de Grouchy, J. T. Banasek, L. Atoyan, T. Byvank, W. M. Potter, J. B. Greenly, D. A. Hammer, and B. R. Kusse are with the Laboratory of Plasma Studies, Cornell University, Ithaca, NY 14853 USA.

J. Engelbrecht is with the Laboratory of Plasma Studies, Cornell University, Ithaca, NY 14853 USA, and also with the Plasma Physics Division, Naval Research Laboratory, Washington, DC 20375 USA.

S. A. Pikuz and T. A. Shelkovenko are with the Laboratory of Plasma Studies, Cornell University, Ithaca, NY 14853 USA, and also with the Lebedev Institute of Physics, 119333 Moscow, Russia.

E. Kroupp, A. Fisher, and Y. Maron are with the Weizmann Institute of Science, Rehovot 76100, Israel.

Color versions of one or more of the figures in this paper are available online at http://ieeexplore.ieee.org.

Digital Object Identifier 10.1109/TPS.2018.2873663

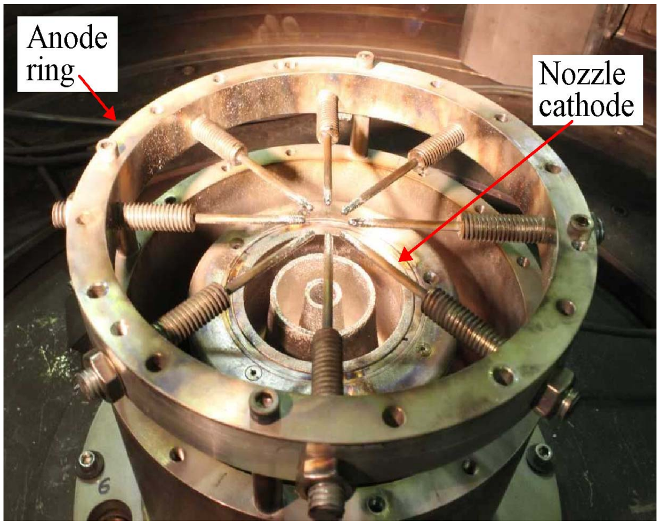


Fig. 1. Triple-nozzle gas-puff z-pinch load on COBRA.

growth of the MRT instability is suppressed. With proper gas profiles, high compression ratios and more or less the same X-ray radiation yields have been achieved as have been seen in the 100-ns implosions [14]–[17].

On COBRA, 200-ns, 0.9-MA implosions with two concentric annular gas puffs and an on-axis wire have been reported in [18] and [19]. In this paper, we present Ar z-pinch studies with a triple-gas puff z-pinch load. In the triple-gas puff loads, a center gas jet has replaced the on-axis wire. The gas pressures in the plena of each nozzle are independently adjusted to give the flexibility in tailoring the radial gas density profile. In the implosion, the outer gas puff region appears to carry the current as it is the preferred low-inductance electrical path. It implodes onto the inner gas puff. The implosion is deaccelerated by the relatively denser inner puff so that the MRT instability growth is suppressed. The center jet plasma is first preheated by a converging shock wave as the imploding plasma approaches the axis. It is then heated quasi-adiabatically until the pinch stagnates [20]. Stable implosions make a tight, pinched plasma and produce intense Ar K-shell X-ray radiation. The center jet adds more ions in the stagnated plasma. In ~100-ns implosion time z-pinches such as on Z, increasing in the Ar K-shell radiation is limited with a center jet [21]. However, in 200-ns implosion time z-pinches, the center jet has significantly enhanced Ar K-shell radiation yields on Double EAGLE, DQ, and Saturn [14]–[16]. In our experiments on COBRA, with an outer-to-inner nozzle plenum pressure ratio of ~1:3, an Ar K-shell yield of ~100 J is produced with the center jet plenum pressure in a range of 10–14 psia.

The remainder of this paper is organized as follows. Section II describes the experiments; Section III presents the experimental results and discusses the effects of the center jet pressure, and the implosion time on the Ar K-shell yields; and Section IV summarizes our conclusions and plans for future experiments.

## II. EXPERIMENTS

Fig. 1 shows the z-pinch load region with the triple-nozzle gas puff assembly. Gas puffs are ejected from the cathode of

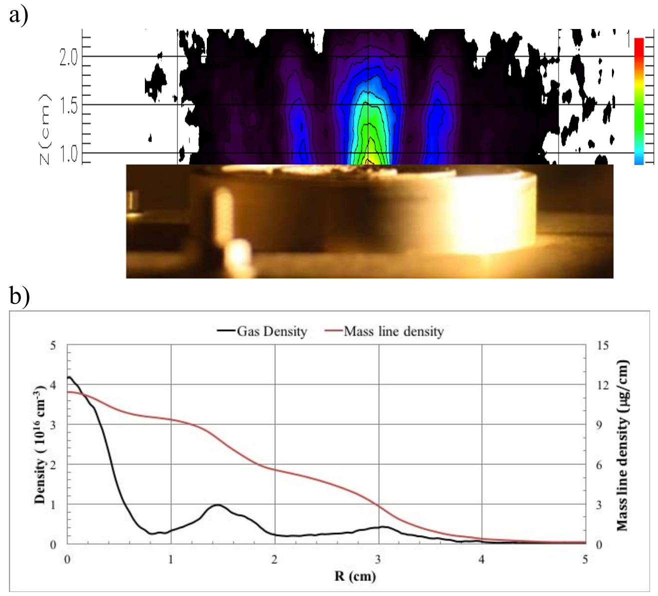


Fig. 2. (a) 2-D density profile measured from PLIF. b) Plot of density (black) and radially integrated mass (red) profile at $z = 1$ cm. The gas pressures in the outer, inner, and center nozzle plena are 0.9, 2.9, and 10 psia, respectively.

COBRA with a gas density rise time of ~500 $\mu$s. The gap between the anode and cathode is 2.5 cm. The return current path consists of eight radial tungsten rods supported by a 20-cm-diameter anode ring. This ring is mounted on four 1-cm-diameter posts connected to the ground side of COBRA.

At the cathode exit plane, the inner and outer diameters of the nozzles are: 6.2 and 4.2 cm for the outer nozzle and 3.6 and 1.4 cm for the inner nozzle. The opening diameter of the center jet nozzle is 1 cm. We have measured the initial gas-puff density profiles using off-site planar laser-induced fluorescence (PLIF) [22]. A 2-D density contour from the measurements is shown in Fig. 2(a). Fig. 2(b) shows a line plot of the density (black) and radially integrated mass at $z = 1$ cm downstream of the nozzle. The plena pressures for the outer, inner, and the jet are 0.9, 2.9, and 10 psia, respectively. The total mass line density is about 11.5 $\mu$g/cm. The outer gas puff has a mass line density of 5.5 $\mu$g/cm and is radially distributed between $R = 2.1$ and 3.8 cm with a peak at $R = 3.1$ cm. The inner puff has 4.0 $\mu$g/cm between 0.8 and 2.1 cm with a peak at 1.4 cm. The mass line density in the center jet is peaked on the axis, and has 2 $\mu$g/cm within a radius of 0.8 cm. Since the implosion time is proportional to the radius times the square root of the mass, the mass in the outer and inner puffs dominate the implosion dynamics.

A set of standard diagnostics were employed on COBRA to characterize the z-pinches from the initial gas phase, through implosion to the final stagnation phase. Fig. 3 shows the arrangement of the plasma diagnostics. A three-frame laser shearing interferometer (LSI) was used to measure the plasma density profile during the implosions [23], [24]. Two four-frame, 4-ns gated, extreme ultraviolet (XUV) cameras captured images of the imploding and stagnated plasma. Filtered pin-hole cameras recorded the X-ray images during stagnation. A 25-$\mu$m Cu filtered p-i-n diode measured hard X-ray

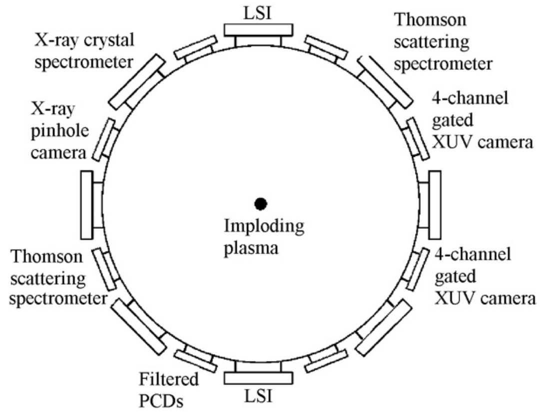


Fig. 3. Arrangement of the vacuum chamber viewports for various plasma diagnostics.

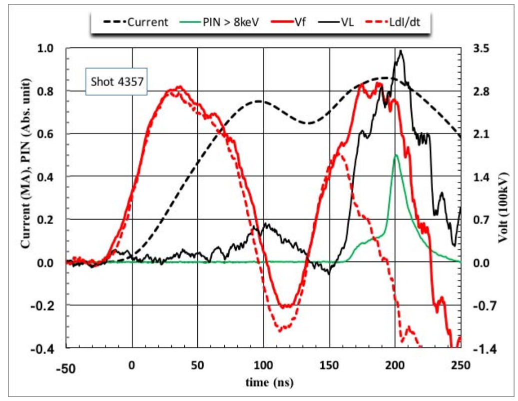


Fig. 4. Typical current and voltage pulses in a z-pinch shot. Black dashed line: current. Red solid line: voltage measured at feed, $V_f = d/dt\ (IL)$. Red dotted line: corresponding *LdI/dt* voltage. Black line: load voltage of $d(L_p I)/dt$. Green line: hard X-ray (>8 keV) emission.

radiation >8 keV. Photoconducting diamond detectors (PCDs) with 25-$\mu$m Be and 12-$\mu$m Ti filters were used for >1 keV and Ar K-shell (>3 keV) X-ray emission, respectively. An unfiltered PCD has a constant response with the photon energies from 2 to 6 keV [25]. One of the PCDs has been cross-calibrated with a known calibration factor PCD. With a 12-$\mu$m Ti filter and 350-V bias, the sensitivity of the cross calibrated, the surface area of 1 mm × 3 mm, PCD is $5.8 \times 10^{-4}$ A/W. At a location 90 cm away from the X-ray source, the calibration factor is $1.17 \times 10^8$ W/V or $1.17 \times 10^8$ J/V-s when terminated into 50 Ω. A spatially resolving spherical mica crystal spectrometer was used to measure the imploding plasma K-shell X-ray spectra. A 5-ns gated Thomson scattering system with an 18-fiber optical bundle was used for temperature and implosion velocity measurements. An X-ray streak camera was used to observe the dynamics of the X-ray production during stagnation. Some of these measurements have been discussed in [26] and [27], and details of the others are being prepared for publishing later.

## III. Experiment Results and Discussion

The goal of these experiments was to achieve stable implosions as well as intense Ar K-shell X-ray radiation using 200-ns rise time current pulses. In ~100-ns implosions, single-nozzle Ar gas puff loads have been optimized for Ar K-shell radiation yields at an initial puff radius of ≤2 cm [28], [29]. Our inner shell is initially at a 2.1-cm radius so, using this result, we have designed our experiment so that the inner shell should implode in ~100 ns. This is accomplished by adjusting our outer and inner nozzle plenum pressures so that the outer shell initially carries the current for ~100 ns before it reaches the inner shell. When the outer puff implodes on the inner, the implosion is slowed down by the denser inner puff mass. Suppressing the MRT instability was observed [30]. The combined outer/inner shells then imploded onto the center puff in <100 ns. To produce these ~200-ns implosions, we found that the line densities should be 5 and 4 $\mu$g/cm in the outer and inner shells, respectively. This corresponds to a ~1:3 ratio of the outer (0.9 psia) and inner (2.7 psia) nozzle plena pressures. With this 1:3 ratio as the condition for a stable implosion, the mass in the center jet was varied by adjusting its plenum pressure up to 22 psia for the most intense Ar K-shell radiation yields. As measured with PLIF, the line mass density of the center jet is 2 $\mu$g/cm at a plenum pressure of 10 psia. This mass density is expected to vary linearly with the plenum pressure.

The CORBA pulse power generator consists of two modules (north and south). Synchronizing the power from the two modules produces a single-peak current pulse with a ~100-ns rise time to peak. Delaying the pulse of the south module by ~100 ns with respect to the north results in a current waveform that has two peaks with an overall rise time to a peak of ~200 ns. Fig. 4 shows the current (black dashed line), applied upstream feed voltage ($V_f$, red solid line), inductive voltage *LdI/dt* (red dotted line), and the load voltage applied to the gas puff plasma $V_L$ (black line). The fixed inductance of the feed and the initial plasma inductance, $L$, are taken to be ~22 nH. The feed voltage $V_f$ was measured by using an inductive voltage monitor. Two peaks appear in the feed voltage with a separation of ~150 ns. They have about the same peak value of ~280 kV, which is over 40% reduction of the >500 kV that accompanies a 100-ns current pulse. Subtracting the inductive voltage *LdI/dt* from $V_f$, the load voltage, $V_L = V_f - LdI/dt = d(IL_p)/dt$, is derived, where $L_p$ is the time-dependent plasma inductance. The load voltage starts to decrease at $t = 100$ ns and peaks again at $t = 205$ ns. Hard X-rays (>8 keV, green line) start to emit at $t = 170$ ns when the load voltage is >100 kV. The initial X-rays are from the high-energy beams in the load region, and later from the pinch plasma with a fast rise time peaking at $t = 200$ ns. By properly adjusting the delay time of the south MARX module, the second current peak is higher than the first and occurs ~200 ns after the current starts to flow. We concentrated on implosions with this two-peak, 200-ns current pulse because it has higher $I^2 dL_p/dt$ input power at the stagnation time.

Fig. 5 shows a typical data set from a 200-ns shot. It includes the current ($I$, black line), load voltage ($V_L$, red line), and hard and Ar K-shell X-ray emission (red dotted and blue lines). The load voltage has huge spikes at the pinch time, which have been smoothed out digitally. The intense X-ray emission occurs about ~10 ns after the peak current.

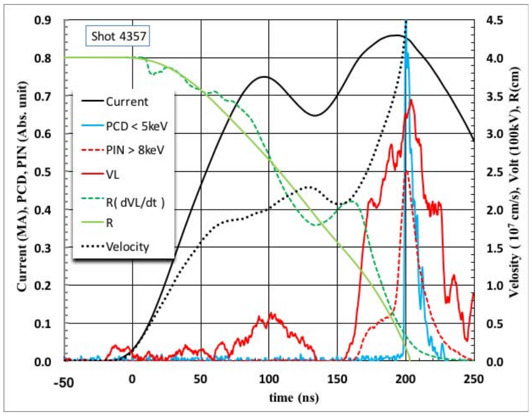


Fig. 5. Typical signals in a z-pinch shot. Black line: current. Red line: $d(L_p I)/dt$ voltage. Red dotted and blue lines: hard and Ar K-shell X-ray emission, respectively. Green solid and green dotted lines: calculated imploding plasma shell radius from the 0-D snowplow model and measured feed voltage pulse, respectively. Black dotted line: velocity from the snowplow model.

During the implosion, there is an inductive z-pinch plasma voltage $V_p (= I dL_p/dt)$, which is due to the motion of the imploding plasma. The z-pinch plasma inductance, $L_p$, is derived from the measured load voltage $V_L$ as

$$V_L = V_f - L\frac{dI}{dt} = \frac{d}{dt}(L_p I) = L_p\frac{dI}{dt} + I\frac{dL_p}{dt}. \quad (1)$$

The z-pinch plasma voltage $V_p$ is proportional to the power delivered to the imploding and pinched plasma [31], [32]. Both hard X-ray and Ar K-shell radiation reach their peak near the peak of $V_L$. The pulsewidth of the Ar K-shell emission is on the order of 10 ns. The imploding plasma radius, shown as the green dotted line in Fig. 5, is derived from the measured feed voltage $V_f$

$$R(t) = R_0 \exp\left\{-\frac{2\pi}{\mu_0 l}\left[\int_0^t \frac{V_L(t')}{I(t)}dt' - L\right]\right\} \quad (2)$$

where $l$ (=0.025 m) is the plasma length, $R_0$ (=4 cm) is the initial plasma radius, and $L_p = \mu_0/(2\pi)\ln(R_0/R)l$. The negative part of the load voltage $V_L$ and the resulting oscillations in the calculated radius about $t = 140$ ns may not be real as the difference between the measured feed voltage $V_f$ and the value of $L\ dI/dt$ being near zero (see Fig. 4). Uncertainties in $V_f$, $dI/dt$, and the value of $L$ cause a large error there.

We also calculated the implosion plasma radius and velocity (green solid line) by using a 0-D snowplow model as

$$m\frac{d^2R}{dt^2} = -\frac{I^2}{R} - \frac{dm}{dR}\left(\frac{dR}{dt}\right)^2 \quad (3)$$

where $R$(cm) is the plasma radius, $t$(ns) is the time, $I$(MA) is the current, and $m$ ($\mu$g/cm) is the area integrated mass line density. With the measured gas density profile (shown in Fig. 2) and current pulse, the radius $R$ (green line) and velocity $dR/dt$ (black dotted line) of the imploding plasma at $z = 1$ cm are derived as shown in Fig. 5. When the plasma implodes onto the edge of the inner gas shell ($R = 2$ cm, $t = 130$ ns), the implosion starts to slow down because it begins sweeping in the mass from the inner shell and because

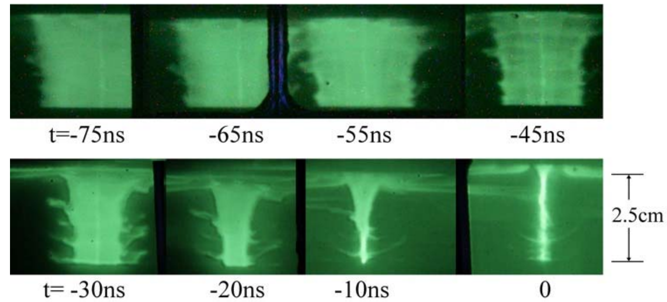


Fig. 6. Gated XUV images, where $t = 0$ is the time of the peak X-ray emission. The cathode is on the bottom. Shot #4731.

the current is falling. The velocity is decreasing until the imploding plasma sweeps through the density peak of the inner puff at $R = 1.5$ cm and $t = 155$ ns. During this deacceleration period, the growth of the MRT instability is suppressed. At the pinch time ($t = 200$ ns), the implosion velocity of $4.5 \times 10^7$ cm/s is achieved. The implosion trajectory derived from the snowplow model is close to the result given by the inductive voltage measurement at the times of $t > 140$ ns and $t > 180$ ns. Between 140 ns $< t <$ 180 ns, these two results for the implosion trajectory start to departure significantly due to the uncertainties in the voltage measurements.

Gated XUV (>20 eV) cameras are used to capture the structure of the imploding plasma. We have observed relatively stable and tightly pinched plasmas as shown in Fig. 6. Measured from the XUV images, the implosion velocity during the time interval of the images was 20–30 cm/$\mu$s. The velocity and imploding plasma radius from the XUV images agree with the snowplow calculations. The diameter of the stagnated plasma was 1 mm as derived from the XUV images.

Fig. 7 shows the raw data from the three-frame LSI (Shot #4354), where a detailed image analysis will be reported in other publications. This LSI is small shift shearing interferometry so the fringe shifts are proportional to plasma density gradients. In Shot #4354, the outer and inner gas puff pressures were doubled to 2 and 6 psia with neon gas, respectively. Argon was kept used in the jet with a pressure of 15 psia. The neon atomic mass is half of the Ar. The initial mass distribution and the corresponding implosion dynamics are expected to be similar to the data presented later. Since the ionization degree of the imploding plasma is also similar, the high initial gas density with neon puffs increases the imploding plasma density and gives more clear fringe shift visibility in the LSI images. The LSI images were taken at times of 70, 60, and 50 ns before stagnation. At these times, the outer and inner plasma shells have merged and are located at radial positions indicated by the red large arrows in Fig. 7. The central jet has been ionized with the plasma density profile similar to its initial gas density, but there is a plasma density spark at the diameters shown by the red small arrows in Fig. 7. The two-vertical green bars indicate the initial location of the center jet. During the 20 ns shown in these images, the combined outer/inner shell is imploding at approximately 20 cm/$\mu$s which is consistent with the snowplow calculations. The smooth boundary indicates a stable implosion. During this

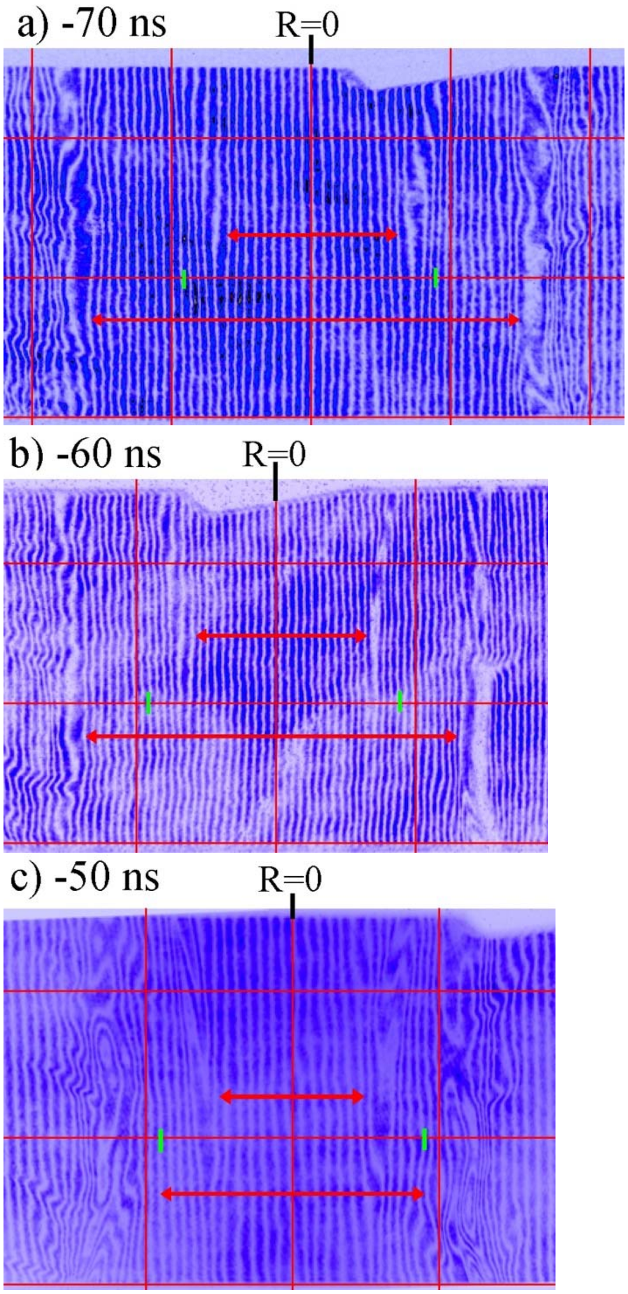


Fig. 7. Laser shearing images of the imploding plasma. The cathode (nozzle exit plane) is on the bottom. The grids are 1 cm apart. The pinch time is at 0. Red long (or short) arrows: position of the combined inner and outer shells (or density spark in the jet). Green vertical bars: outer edge of the central jet Shot #4354.

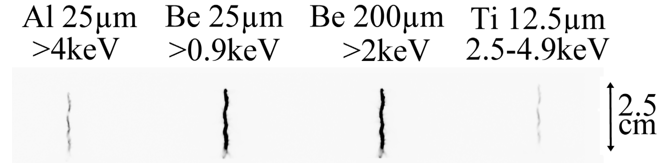


Fig. 8. Pinhole images of the X-rays emitted from the pinch plasma with various filters. The length of the pinch plasma is 2.5 cm. Shot #4346.

TABLE I

PEAK CURRENT ($I$), IMPLOSION TIME ($T$), CENTER JET PLENUM PRESSURE (JET), AND AR K-SHELL RADIATION POWER AND ENERGY (PCD)

| Shot # | I (MA) | T (ns) | Jet (Psia) | PCD (GW) | PCD (J) |
|---|---|---|---|---|---|
| 4339 | 0.86 | 198 | 10 | 4.2 | 63 |
| 4340 | 0.84 | 178 | 4.6 | 0.8 | 20 |
| 4341 | 0.86 | 186 | 4.6 | 3.4 | 60 |
| 4342 | 0.87 | 198 | 10.5 | 5.7 | 85 |
| 4343 | 0.89 | 195 | 14 | 3.8 | 63 |
| 4344 | 0.89 | 204 | 18 | 2.7 | 53 |
| 4345 | 0.89 | 214 | 22 | 0.8 | 35 |
| 4346 | 0.88 | 203 | 14 | 6.5 | 103 |
| 4347 | 0.83 | 211 | 10 | 5.0 | 71 |
| 4349 | 0.87 | 209 | 19 | 1.0 | 41 |
| 4350 | 0.82 | 232 | 19 | 0.9 | 33 |
| 4351 | 0.86 | 209 | 19 | 1.2 | 43 |
| 4352 | 0.86 | 217 | 19 | 0.7 | 38 |

time, the location of the density spark near the central jet has slightly decreased in diameter from 1.8 to 1.6 cm. This preionization of the jet has occurred before the imploding shells have reached the jet and consequently must be the result of shock heating and/or photoionization. The plasma density spark in the jet is only observed in LSI when the jet was at plenum pressures >10 psia, where the plasma density is higher enough to be clearly detected by the LSI.

Fig. 8 shows the filtered pinhole images of the X-ray emission of the stagnated plasma. The filters used were a 25-$\mu$m thick Be foil for X-ray photon energy $E > 0.9$ keV, a 200-$\mu$m Be foil for $E > 2$ keV, a 25-$\mu$m Al foil for $1.4 < E < 1.6$ keV and $E > 4$ keV, and a 12.5-$\mu$m Ti foil for $2.5 < E < 4.85$ keV. The X-ray radiation was distributed along the pinch axis, with clear small amplitude oscillations in radius along the entire plasma column. These correspond to the MRT instabilities and have a wavelength of about 4 mm. The Ar K-shell X-ray radiation, in the images filtered by 12.5-$\mu$m Ti and 25-$\mu$m Al, is about 1 mm in diameter while the emission in the images filtered by the 25 and 200-$\mu$m Be foil is about 1.4 mm in diameter. Varying the jet gas pressure, the pinch plasma diameters and the MTR instability wavelengths remain more or less the same. It suggests that the center jet has no or very limited effects to the MTR instability.

The Ar K-shell X-ray yield was investigated by varying the nozzle plenum pressure of the center jet, while keeping the pressure ratio in the outer and inner plena at ≈1:3. A calibrated PCD was used to measure the Ar K-shell X-ray radiation power. Time integration of the PCD signal gives the total emitted K-shell X-ray energy.

Table I lists the peak currents, implosion times, and the jet pressures in the experiments. The last two columns in Table I are the measured Ar K-shell X-ray powers and energies. In the experiments, the jet plenum pressure was varied from 4 to 22 psia, while the outer and inner gas-puff pressures are kept at 0.9 and 2.9 psia, respectively. The puff mass density varies linearly with the nozzle plenum pressure. At these pressures, the line mass density in the outer puff is 5.5 and 4.0 $\mu$g/cm in the inner puff. The pressure scaling of the mass in the jet is 0.2 $\mu$g/cm psia.

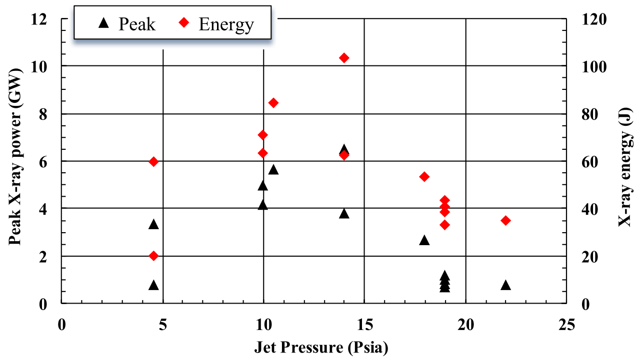


Fig. 9. Peak X-ray (black triangles) and their integrated signals (red diamonds) from the 12-$\mu$m Ti filtered PCD signals versus the jet gas pressure. (Shot #4339-4352).

Fig. 9 is a plot of the peak (black triangles) and the time-integrated (red diamonds) Ar K-shell X-ray signals from the shots listed in Table I. The K-shell radiation power is proportional to the densities of the electrons and the K-shell ions, which are adjusted by the center jet mass. At low jet pressures, less electrons and/or Ar ions are in the stagnated pinch so that the K-shell radiation is lower. At high jet densities, fewer ions can be heated to the K-shell ionization states for emitting K-shell radiation. Therefore, the X-ray power and yield starts to increase as the jet pressure increases from 5 to ~10 psia. The K-shell radiation power and yield reached their peak value of 6.5 GW and 103 J, when the jet pressure is increased to 14 psia. With a further increase in the jet pressure up to 18+ psia, the K-shell radiation power and energy decrease. There is scattering in the K-shell peak power and energy at a given jet pressure. These could be caused by the implosion time as discussed next. Taking into account the shot-to-shot variations, intense Ar K-shell radiation is produced at a jet pressure between 10 and 14 psia. The yield of Ar K-shell X-ray radiation in this jet pressure range is 77 ± 17 J with peak current levels of 0.87 ± 0.02 MA. Therefore, the best performing loads are reasonably well optimized compared to other experiments in the literature.

For a given z-pinch current rise time and gas load configuration, the pinch plasma density is proportional to $I^2$ [4], [33]. With 1-MA implosion currents, the Ar K-shell line radiation is optically thin so that it is proportional to the density squared and therefore scales as $I^4$. At high currents (>3 MA), the Ar becomes optically thick to K-shell radiation. The K-shell emission then comes from a volume determined by the optical path length and surface area. Since the optical path length varies inversely with the density, the K-shell yield becomes proportional to the density, i.e., current scaling is $I^2$. This is an efficient radiation source as the input power is also proportional to $I^2$. Reference [4] has reported that on Double EAGLE at 3.5 MA and 205-ns implosion time, (Shot #5556), the Ar K-shell yield was 21 kJ, and on ZR machine at 15 MA and 100 ns (Shot #2560), it was 363 kJ. The current scaling law for the Ar K-shell goes as $I^2$ from 3.5 to 15 MA. At the 1-MA current level, COBRA is not an efficient Ar K-shell radiation source. Applying the $I^4$ 0.9-/2.9-psia current scaling law, the expected COBRA Ar K-shell yield is 80.2 ± 7.6 J at 0.87 ± 0.02 MA. This agrees with our experimental results of 77 ± 17 J.

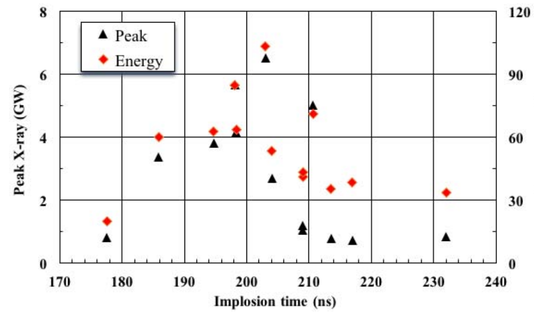


Fig. 10. Peak (black triangles) and yield (red diamonds) of the Ar K-shell X-ray emission versus implosion time.

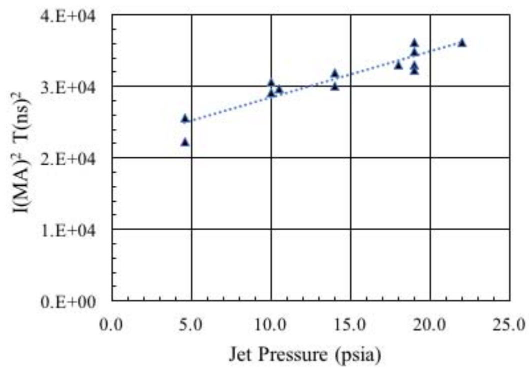


Fig. 11. Implosion time as a function of the center jet plenum pressure.

For the given load/nozzle configuration on COBRA, there is an optimum implosion time for the Ar K-shell X-ray emission. Fig. 10 shows the Ar K-shell radiation peaks (black triangle) and yields (red diamonds) as a function of the implosion time. The optimum implosion time for X-ray yield appears to be slightly greater than 200 ns, the time of peak current in the power pulse. Early implosion time < 190 ns appears to be the result of an under massed puff. The relatively lower plasma density reduces the K-shell radiation. Longer implosion times >210 ns appear to be over massed. In the more massive puffs, the Ar ions have less kinetic energy so that fewer ions are heated to the K-shell ionization state.

The ~200-ns implosion time is mainly determined by the mass in the outer and inner plasma shells. Higher jet pressures slightly increase the implosion time. From the implosion dynamics, the relationship among the peak current ($I$), implosion time ($T$), and mass distribution, is given by

$$I^2T^2 \propto \sum mR^2 = \alpha + \beta P_{\text{jet}} \tag{4}$$

where $\sum mR^2$ is a time-integrated product of the imploding plasma radius squared and its mass, and $\alpha$ and $\beta$ are constants. The mass in the center jet is proportional to the plenum pressure of the center jet $P_{\text{jet}}$. Fig. 11 plots the $I^2T^2$ versus the jet pressure. These fit well to a linear increase with the jet pressure.

## IV. Conclusion

We have studied triple-gas puff Ar z-pinches at ~200-ns implosion times and a current level of ~0.9 MA on COBRA.

A double-peak current waveform was employed in the gas-puff implosions. A set of diagnostic instruments was used to measure the gas-puff z-pinch from initial gas, implosion to the final pinch phase. Stable implosions were achieved with an outer/inner nozzle plenum pressure ratio of $\sim$1:3 and a dense center jet. Preionization of the center jet by the outer/inner imploding plasma due to shock heating or photoionization was observed from the LSI images. The Ar K-shell X-ray emission was optimized by varying the center jet mass. About 100 J, $\sim$10-ns Ar K-shell X-ray emission was produced at outer, inner, and jet plena pressures of 0.9, 2.9, and 10–14 psia, respectively, where the implosion time was $200 \pm 10$ ns. Using the triple-nozzle loads, the long implosion time ($>200$ ns) z-pinches have produced comparable Ar K-shell yields to the 100-ns implosion time shots, which gives a promising path for future high-current-driven plasma radiation source development. Investigation of the implosion dynamics and X-ray production with different driving current waveforms, different diameters of the gas puffs, and/or with an external $B_z$ field will be studied in the future.

## Acknowledgment

The authors would like to thank H. Wilhelm, T. Blanchard, and D. Hawkes for their very important support for the experiments and the COBRA facility operation. They would also like to thank Dr. J. Giuliani, Dr. N. D. Ouart, and Dr. A. Velikovich of the Naval Research Laboratory, Washington, DC, USA, and Dr. R. Spielman at Idaho State University for many valuable discussions on gas-puff Z-pinches.

## References

[1] D. D. Ryutov, M. S. Derzon, and M. K. Matzen, "The physics of fast Z pinches," *Rev. Mod. Phys.*, vol. 72, no. 1, p. 167, 2000.

[2] C. Deeney, C. A. Coverdale, and M. R. Douglas, "A review of long-implosion-time z pinches as efficient and high-power radiation sources," *Laser Part. Beams*, vol. 19, no. 3, pp. 497–506, Jul. 2001.

[3] M. G. Haines, "A review of the dense Z-pinch," *Plasma Phys. Controlled Fusion*, vol. 53, no. 9, p. 093001, 2011.

[4] J. L. Giuliani and R. J. Commisso, "A review of the gas-puff Z-pinch as an X-ray and neutron source," *IEEE Trans. Plasma Sci.*, vol. 43, no. 8, pp. 2385–2453, Aug. 2015.

[5] D. J. Ampleford *et al.*, "Contrasting physics in wire array z pinch sources of 1-20 keV emission on the Z facility," *Phys. Plasmas*, vol. 21, no. 5, p. 056708, 2014.

[6] C. Deeney *et al.*, "Enhancement of X-Ray power from a Z pinch using nested-wire arrays," *Phys. Rev. Lett.*, vol. 81, no. 22, p. 4883, 1998.

[7] C. L. Hoyt *et al.*, "Cable array Z-pinch experiments at 1 MA," *IEEE Trans. Plasma Sci.*, vol. 40, no. 12, pp. 3367–3371, Dec. 2012.

[8] H. Sze *et al.*, "Efficient argon K-shell radiation from a Z pinch at currents >15 MA," *Phys. Plasmas*, vol. 8, no. 7, p. 3135, 2001.

[9] C. A. Coverdale *et al.*, "K-shell X-ray sources at the Z accelerator," *High Energy Density Phys.*, vol. 6, no. 2, pp. 143–152, Jun. 2010.

[10] B. Jones *et al.*, "The effect of gradients at stagnation on K-shell X-ray line emission in high-current Ar gas-puff implosions," *Phys. Plasmas*, vol. 22, no. 2, p. 020706, 2015.

[11] M. R. Gomez *et al.*, "Experimental study of current loss and plasma formation in the Z machine post-hole convolute," *Phys. Rev. Accel. Beams*, vol. 20, no. 1, p. 010401, 2017.

[12] B. H. Failor *et al.*, "Axially resolved z-pinch density, electron temperature, and K-shell emitting mass estimates from charge-coupled device based diagnostics," *Rev. Sci. Instrum.*, vol. 72, no. 1, pp. 1232–1235, Jan. 2001.

[13] A. L. Velikovich, F. L. Cochran, and J. Davis, "Suppression of Rayleigh-Taylor instability in Z-pinch loads with tailored density profiles," *Phys. Rev. Lett.*, vol. 77, no. 5, p. 853, 1996.

[14] H. Sze *et al.*, "Efficient radiation production in long implosions of structured gas-puff Z pinch loads from large initial radius," *Phys. Rev. Lett.*, vol. 95, no. 10, p. 105001, 2005.

[15] J. S. Levine *et al.*, "Implosion dynamics and radiative characteristics of a high yield structured gas puff load," *Phys. Plasmas*, vol. 13, no. 8, p. 082702, 2006.

[16] R. J. Commisso *et al.*, "Overview of 12-cm-diameter, argon gas-puff experiments and analyses with >200-ns implosion times at 3- to 6-MA peak currents," in *Proc. 7th Int. Conf. Dense-Z Pinches, AIP Conf.*, vol. 1088, D. A. Hammer and R. B. Kusse, Eds. Melville, NY, USA: American Institute Physics, 2009, pp. 233–238.

[17] P. L. Coleman *et al.*, "Recent results for large diameter (12 cm) gas puff Z-pinches at peak currents of >3 to <6 MA," in *Proc. Dense Z-Pinches, 6th Int. Conf. Dense Z-Pinches, AIP Conf.*, vol. 808, 2006, pp. 163–168.

[18] N. Qi *et al.*, "Study of gas-puff Z-pinches on COBRA," *Phys. Plasmas*, vol. 21, p. 112702, Sep. 2014.

[19] J. T. Engelbrecht *et al.*, "Enhancing the X-ray output of a single-wire explosion with a gas-puff based plasma opening switch," *Phys. Plasmas*, vol. 25, no. 2, p. 022704, 2018.

[20] A. S. Chuvatin, L. I. Rudakov, A. L. Velikovich, J. Davis, and V. I. Oreshkin, "Heating of on-axis plasma heating for keV X-ray production with Z-pinches," *IEEE Trans. Plasma Sci.*, vol. 33, no. 2, pp. 739–751, Apr. 2005.

[21] A. J. Harvey-Thompson *et al.*, "Investigating the effect of adding an on-axis jet to Ar gas puff Z pinches on Z," *Phys. Plasmas*, vol. 23, no. 10, p. 101203, Oct. 2016.

[22] N. Qi, B. H. Failor, J. Banister, J. S. Levine, H. M. Sze, and D. Lojewski, "Two-dimensional gas density and velocity distributions of a 12-cm-diameter, triple-nozzle argon Z-pinch load," *IEEE Trans. Plasma Sci.*, vol. 33, no. 2, pp. 752–762, Apr. 2005.

[23] N. Qi *et al.*, "Z pinch imploding plasma density profile measurements using a two-frame laser shearing interferometer," *IEEE Trans. Plasma Sci.*, vol. 30, no. 1, pp. 227–238, Feb. 2002.

[24] S. A. Pikuz *et al.*, "A simple air wedge shearing interferometer for studying exploding wires," *Rev. Sci. Instrum.*, vol. 72, no. 1, p. 1098, 2001.

[25] R. B. Spielman, "Diamond photoconducting detectors as high power z-pinch diagnostics," *Rev. Sci. Instrum.*, vol. 66, no. 1, p. 867, 1995.

[26] N. D. Ouart *et al.*, "Radiative properties of argon gas puff z-pinch implosions on COBRA," *Phys. Plasmas*, vol. 23, no. 10, p. 101202, 2016.

[27] S. V. R. Rocco, J. T. Banasek, W. M. Potter, B. R. Kusse, and D. A. Hammer, "Time-resolved Thomson scattering on gas-puff Z-pinch plasmas at pinch time," *IEEE Trans. Plasma Sci.*, vol. 46, no. 11, Oct. 2018.

[28] C. Deeney *et al.*, "Increased kilo-electron-volt X-ray yields from Z-pinch plasmas by mixing elements of similar atomic numbers," *Phys. Rev. E, Stat. Phys. Plasmas Fluids Relat. Interdiscip. Top.*, vol. 51, no. 5, p. 4823, 1995.

[29] J. L. Giuliani *et al.*, "Plasma pinch research on University pulsed-power generators in the United States," *IEEE Trans. Plasma Sci.*, vol. 40, no. 12, pp. 3246–3264, Dec. 2012.

[30] P. W. L. de Grouchy *et al.*, "Observations of the magneto-Rayleigh-Taylor instability and shock dynamics in gas-puff Z-pinch experiments," *Phys. Plasmas*, vol. 25, no. 7, p. 072701, 2018.

[31] D. P. Murphy *et al.*, "Time-resolved voltage measurements of z-pinch radiation sources with a vacuum voltmeter," *Rev. Sci. Instrum.*, vol. 79, no. 10, p. 10E306, 2008.

[32] G. C. Burdiak *et al.*, "Determination of the inductance of imploding wire array Z-pinches using measurements of load voltage," *Phys. Plasmas*, vol. 20, p. 032705, Mar. 2013.

[33] J. W. Thornhill, K. G. Whitney, J. Davis, and J. P. Apruzese, "Investigation of K-shell emission from moderate-Z, low-$\eta$ (-velocity), Z-pinch implosions," *J. Appl. Phys.*, vol. 80, no. 2, p. 710, 1996.

Authors' photographs and biographies not available at the time of publication.